Rayleigh scattering and redistribution of radiation in He I plasmas: Measurements and calculations

P. Drepper, S. Ferri, S. Maurmann, and H.-J. Kunze
Institute for Experimental Physics, Ruhr University Bochum, 44780 Bochum, Germany
(Received 8 June 2001; revised manuscript received 25 February 2001; published 10 October 2002)

Conditions for which Rayleigh scattering and redistribution of radiation can be observed are examined. The competition between the relaxation processes and spontaneous emission is shown to determine the conditions for partial redistribution. We investigate specific cases in the singlet and triplet He I atomic system for plasma parameters reachable experimentally in a well diagnosed magnetic multipole source. Partial redistribution on the $2\,^1S-4\,^1P$ at 396.5 nm, $2\,^1P-5\,^1D$ at 438.8 nm, $2\,^3P-5\,^3D$ at 402.6 nm, $2\,^3P-4\,^3D$ at 447.2 nm and $2\,^3P-4\,^3S$ at 471.3 nm fine structure transitions is observed employing a dye laser pumping the He I plasma. We make use of a previously developed two-photon formalism based on the frequency fluctuation model to calculate radiative redistribution functions. Results of the partial redistribution measurements are presented, augmented by a comparison with calculations. This allows us to confirm available electron-atom elastic collision rates to within 20%.

DOI: 10.1103/PhysRevE.66.046404 PACS number(s): 52.25.Os, 32.70.Jz, 34.50.Fa, 34.10.+x

I. INTRODUCTION

Knowledge of how an atom scatters radiation is important in many fields of plasma physics. In astrophysics, the theory of radiative transfer in spectral lines has a long history [1–5] and is of significant importance in determining the structure of many astrophysical systems. In order to determine the emission coefficient, needed to solve the equation of transfer, scattering of radiation can be important and hence the concept of redistributed radiation $I(\omega_P,\omega_S)$ is introduced. The latter relates the spontaneously emitted radiation at frequency ω_S to the incident radiation of frequency ω_P. Its knowledge is also of importance in the calculation of optical depths, on which x-ray diagnostics of high-Z, high-density plasmas, for example, depend [6,7].

The first spatially resolved observation of light scattered by an atomic vapor near a resonance line and the first experimental study of the redistribution of light by collisions as a function of the detuning of the incident light have been reported by Carlsten and Szöke in 1976 [8]. The pattern of coherently scattered and redistributed radiation has also been observed only under very few experimental conditions for neutral emitters in plasmas due to the experimental difficulties [9–11].

In the meantime, redistribution of radiation has been studied using several theoretical approaches. The most common approximation for its calculation, complete redistribution, assumes that the emission profile has the same shape as the fluorescence profile, so that the redistribution function becomes a product of the absorption and fluorescence functions. For the conditions of an arc plasma this is valid because the spontaneous emission rate can be neglected with respect to the other damping rates in the plasma. Nevertheless, different inhomogeneous line-broadening mechanisms, such as the Doppler effect arising from thermal motion and broadening due to collisions of the radiating atoms with the nearby particles, can result in partial redistribution. In its rest frame, an atom undergoing collisions can, for photons with frequencies close to the resonance transition, either scatter photons coherently, i.e., $\omega_P=\omega_S$, or redistribute the emission about the resonance frequency. The former process gives rise to the Rayleigh peak, the latter to the fluorescence peak. An important advance in the study of such processes has been achieved by Omont and co-workers [5], who investigated this for a two- and a three-level atom by using the quantum mechanical description of matter and radiation. Recently a more sophisticated model for the calculation of radiative redistribution function has been developed by Mossé *et al.* [12]. This model permits the investigation of radiative redistribution processes for complex emitters and in a wide range of plasma conditions and constitutes a powerful tool for the study of radiative transport in plasmas.

Experiments such as those discussed in Ref. [13], where partial redistribution is predicted because of the fine structure inhomogeneity, are of general interest due to the possibility of testing models in the line shape theory. As an example, for the study of the ion dynamics effect, redistribution provides a more sensitive probe than the linear response [12]. A second example of what a critical redistribution experiment could provide is found in the basic assumption that the inelastic electron-atom collisions can be ignored. Those effects would be emphasized in the redistributed line shape, and thus comparisons between models and such respective experiments would lead to a measurement of inelastic collisions rates. Unfortunately, experimental difficulties have so far impeded such studies.

This paper deals with Rayleigh scattering and redistribution of radiation in He I plasmas, which are not only theoretically but also experimentally investigated in a magnetic multipole plasma source using a dye laser for pumping the plasma [14]. In Sec. II, we consider a simplified picture to examine qualitatively the occurrence of partial redistribution. With the use of the analytical expression of Omont, Smith and Cooper [5], we show how the competition between spontaneous emission and collisions (electron-atom) affects the redistribution of radiation. We have distinguished five cases of interest, depending on which one of those damping

rates dominates. This drives our choice of the selection of fine structure transitions in the triplet and singlet system of He I, that can be observed experimentally. Section III is devoted to the description of the experiment. After presenting the experimental setup, which consists of the plasma source, the laser system and the detection unit, we present the characteristics of the plasma parameters. Spatially resolved, radial and axial measurements of electron density and electron temperature show that the plasma source is particularly stable and thus well suited for the studies of the redistribution. We also present in this section the operation of the plasma source for the redistribution of radiation with all the technical difficulties connected with such measurements. The theoretical model used to calculate the redistribution of radiation is discussed in Sec. IV. The frequency fluctuation model (FFM) [15,16], which has been successfully used to provide complex ionic absorption or emission spectral line shapes for emitters in a wide range of plasma conditions, has been extended to enable calculations of the radiative redistribution [12]. The system of dressed two-level emitters or Stark dressed transitions defined in the FFM includes inhomogeneities of the line broadening process, and constitutes the most important simplification permitting a straightforward extension to the two-photon process. As an illustration, we present the calculations of the scattered spectra of the He I $2\,^3P$–$5\,^3D$ transition. Finally, the observed scattered spectra are presented in Sec. V, with comparisons with the theoretical spectra.

II. SKETCH OF THE SPECTRUM FOR A TWO-LEVEL SYSTEM

When a monochromatic light wave impinges on an atom near one of its resonance lines, part of the light is scattered. To give a qualitative description of such a process, the familiar two-level system will be considered in this section. The level scheme and the relaxation rates are displayed in Fig. 1, where the pumping radiation at the frequency ω_P is represented by the double line. The spontaneous decay rates of lower and upper levels, Γ_a and Γ_b, respectively, are represented by wavy lines and collisional rates $\gamma_{e,a,b}$ by single lines. Elastic collisions are usually viewed as collisions which interrupt the phase of the emitted wave train. However, in the present context, elastic collisions (γ_e in Fig. 1) are considered as collisions which transfer population from the laser-excited virtual level (level in dots in Fig. 1) to the real upper level *b*. In contrast to this, inelastic collisions ($\gamma_{a,b}$ in Fig. 1) are those events which cause a net population transfer from the lower and upper levels to other levels.

In the absence of elastic collisions and of Doppler effects, the spectrum of the scattered light is a single line centered on the incident frequency, known as Rayleigh scattering. With elastic collisions present, population can be transferred to the real upper level and the emitted radiation is divided between the Rayleigh line and the fluorescence line emitted near the resonance frequency. This is the case of partial redistribution. For a homogeneously broadened line, the amplitude of the Rayleigh line depends on the ratio of the spontaneous emission rate (of the upper level) and the elastic collision rate,

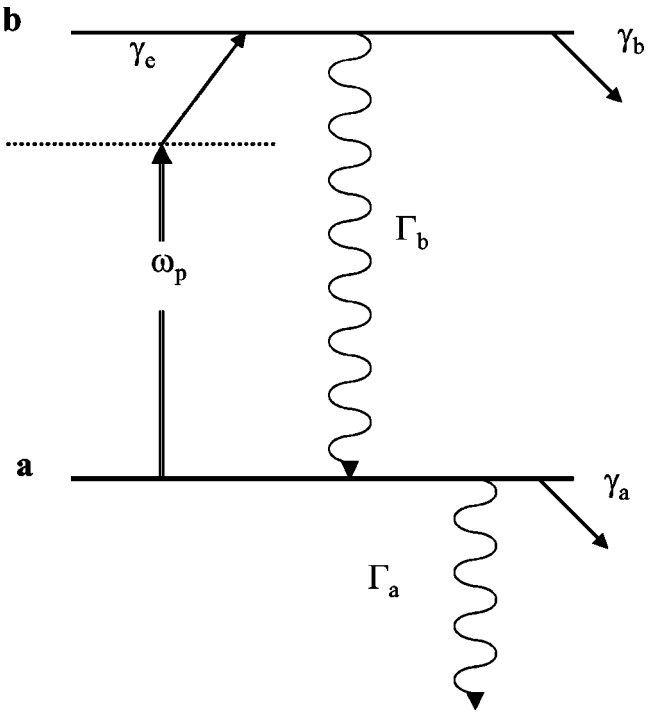

FIG. 1. Parameters for the two-level system.

and its width depends on the decay rates of the lower level, i.e., on the spontaneous emission rate and the inelastic collision rate of the lower level. In order to have complete redistribution the fluorescence line must dominate. The occurrence of partial or complete redistribution is closely related to the competition between all those damping rates. They determine the magnitude of the correlation between the pumping radiation and that emitted spontaneously by the radiator. As illustration we make use of the power spectrum, $I(\omega_P,\omega_S)$, of the radiation emitted at a frequency ω_S by a system pumped at a frequency ω_P. Its calculation is a complex problem due to the atomic system of the emitter and the broadening mechanisms (homogeneous and inhomogeneous) [17]. Nevertheless, analytical expressions exist in the scheme of Fig. 1. In order to illustrate the role of all the above damping rates on the radiative redistribution, we make use of the well known expression proposed by Omont, Smith, and Cooper [5], which is valid whenever the impact theory is valid, i.e., whenever the frequency differences are less than $1/\tau_c$ where τ_c is the duration of typical collisions:

$$I(\omega_P,\omega_S)=Af(\omega_P)\left\{\frac{\Gamma_b(\gamma_{ba}+\gamma_{t,a})}{4\gamma_{ba}^2}\right.$$
$$\times f(\omega_S)\frac{\gamma_{t,a}}{(\omega_P-\omega_S)^2+\gamma_{t,a}^2}$$
$$+\left(\frac{\Gamma_b}{4\pi\gamma_{ba}}\right)\left[1+\frac{f(\omega_S)}{f(\omega_P)}\right]$$
$$\left.+\frac{\Gamma_b(4\gamma_{ba}-2\gamma_{t,b}\gamma_{ba}-\gamma_{t,b}\gamma_{t,a})}{4\gamma_{t,b}\gamma_{ba}^2}\right\}, \quad (1)$$

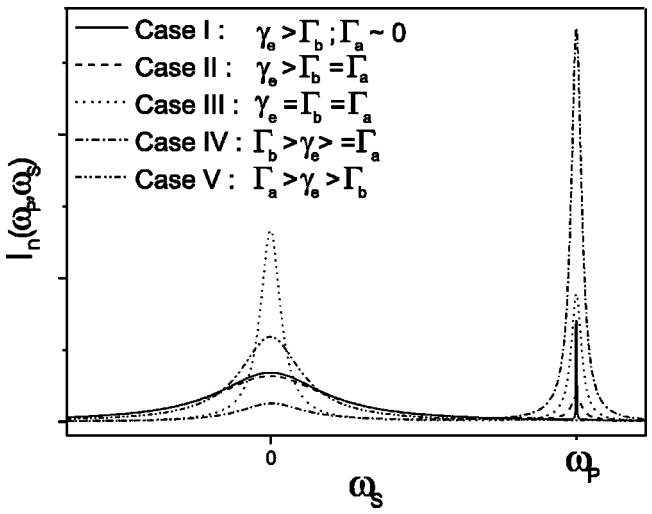

FIG. 2. Examples of scattered emission calculated with the use of OSC's expression [5] for different cases. ω_S is in arb. units and the integrated emission is normalized to 1.

where f denotes the Lorentzian emission or absorption profile,

$$f(\omega)=\frac{(\gamma_{ba})/\pi}{(\omega-\omega_0)^2+\gamma_{ba}^2}, \tag{2}$$

and $\gamma_{ba}=\gamma_e+[(\Gamma_a+\Gamma_b)/2]+[(\gamma_a+\gamma_b)/2]$ and $\gamma_{t,i}=\Gamma_i+\gamma_i$. The constant A is a normalization coefficient. The occurrence of partial redistribution depends critically upon the competition of the rates of spontaneous emission and elastic collisions. In Fig. 2, we have plotted $I_n(\omega_P,\omega_S)$ calculated for different assumed cases with A chosen such that $\int\int I_n(\omega_P,\omega_S)d\omega_P d\omega_S=1$: variation of the different damping rates allows one to identify conditions for which Rayleigh scattering and redistribution of radiation can be observed, and to see which of the two scattered processes dominates. Nevertheless, we neglect inelastic collisions in the calculations, since we cannot isolate their effects experimentally; they essentially broaden the profile, which is not seen anyway because the profile width is instrumental. We distinguish five cases of interest.

(1) The lower state has zero width ($\gamma_{t,a}\sim 0$), i.e., the lower state is the ground state or a metastable state; the redistribution is caused solely by elastic collisions. This corresponds to case I on Fig. 2, where the Rayleigh peak centered on ω_P can be described with a δ function.

(2) The lower state has a width of the order of that of the upper level. Three cases of partial redistribution can be observed: the elastic collision rate is larger than the spontaneous emission rate of the upper level, the fluorescence line will dominate (case II in Fig. 2). All rates are of the same order of magnitude; the scattered profile shows both fluorescence line and Rayleigh peak (case III in Fig. 2). Finally, the spontaneous rate is larger than the elastic collision rate; the Rayleigh peak will dominate (case IV in Fig. 2).

TABLE I. He I transitions of interest and their characteristics.

Transition	λ(nm)	$\Gamma_b(s^{-1})$	$\gamma_e(s^{-1})$	Corr. theor. case
$2\,^1S$–$4\,^1P$	396.5	6.83×10^6	4.80×10^7	I
$2\,^3P$–$5\,^3D$	402.7	1.16×10^7	6.28×10^7	II
$2\,^3P$–$4\,^3S$	471.3	9.30×10^6	4.35×10^6	III
$2\,^3P$–$4\,^3D$	447.2	2.46×10^7	7.25×10^6	IV
$2\,^1P$–$5\,^1D$	438.8	9.04×10^6	8.46×10^7	V

(3) The lower state has a significant decay rate (case V in Fig. 2); we can still observe redistribution, even in the absence of elastic collisions [10]. It can happen when radiation from the lower level is trapped due to optical thickness of the transition. This would cause repopulation of the lower level.

We investigated fine structure transitions of He I in order to match these five cases. The choice was driven not only by phenomenological interest but also by experimental observability. One has to choose sufficiently bright transitions, i.e., coming from not too high principal quantum numbers, but having an upper level significantly broadened by collisions for the given plasma parameters. In addition, the wavelength window of the transitions has to match the best gain of the pumping laser. One also has to take care of the choice of the lower level in order to have a non-negligible spontaneous decay compared to the upper one, but still to have sufficient population on this lower level. All those compromises lead to our choice of five fine structure transitions in the singlet and triplet system of He I. The transitions of interest and their characteristics are shown in Table I. The spontaneous emission rates Γ_a and Γ_b are taken from Theodosiou [18]. The elastic electron-He collision rates γ_e are calculated for the present experimental plasma parameters ($N_e=10\times10^{12}$ cm^{-3} and $kT_e=5$ eV) using the impact theory [19]. In the present study electron-atom collisions dominate all other collision processes due to a high ionization degree of the helium plasma of about 1%. An estimation made by using the cross sections given in [20] shows that, for the present plasma conditions, the He I–He collision rate is 10^5 times lower than the electron-He collision rate. Due to the lower population densities in the excited states, respective collision rates are even much smaller. In the triplet system, we choose to pump from the level $2\,^3P$ which has a spontaneous emission rate non-negligible compared to the others ($\Gamma_{2^3P,2^3S}=1.02\times10^7$ s^{-1}), but which is sufficiently populated to be pumped.

Measurements of the population density N_{2^3P} of the $2\,^3P$ state were performed with the present experimental setup employing Rayleigh scattering at some detuning from the line center to check the feasibility of redistribution measurements. A population density of 3.3×10^{10} cm^{-3} was found for our plasma conditions. This is consistent with former experiments of Lokaczyk [21]. Concerning the choice of lower levels in the singlet system, previous measurements of the population density of the $2\,^1S$ state convinced us to choose this state [21]. In addition the $2\,^1P$ level is reasonably populated because of the high optical depth of the resonance transition.

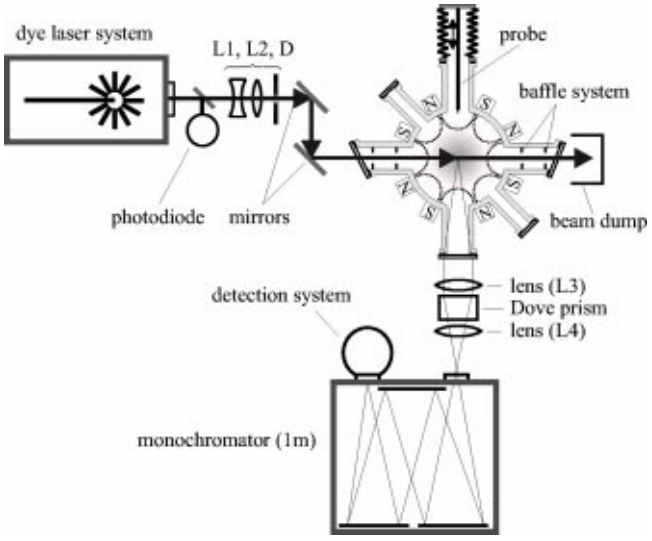

FIG. 3. Experimental setup.

III. DESCRIPTION OF THE EXPERIMENT

A. Experimental setup

The experimental setup used for the investigation of Rayleigh scattering and redistribution of radiation in a helium plasma is shown in Fig. 3. The main parts are the plasma source, the laser system, and the detection unit. The helium plasma is produced in a magnetic multipole plasma source which has been described previously in detail [22]. Briefly, the anode of the plasma source is a vertically mounted cylindrical vessel (diameter $d=15$ cm, length $l=33$ cm) made of nonmagnetic stainless steel. To diagnose the plasma there are four ports with windows ($d=3.5$ cm) on each of three levels and two ports with windows ($d=1.0$ cm) on each of two levels at the periphery of the discharge chamber. The upper and lower ends of the vessel are formed conically with two ports ($d=3.5$ cm) for the gas inlet and for the cathode mount, respectively. The directly heated cathode-filament is a small tube (1/4 in. in diameter and 1 in. in length) consisting of lanthanum-hexaboride (LaB_6). A magnetic octopole structure (longitudinal line cusp configuration) on the vessel's external wall is used for the plasma confinement. The radial magnetic induction at the inner wall of the discharge chamber ($r=7.5$ cm) in front of the magnets is $B_r=250$ mT and at the position of the ports $B_r=60$ mT, decreasing rapidly to a value of $B_r=20$ mT at $r=3$ cm. Close to the source-center starting at $r\approx 1$ cm the magnetic field is negligible.

The laser system consists of a dye laser (Lambda Physik LPD 3002E) which is pumped by an excimer laser at a wavelength of 308 nm (Lambda Physik LPX 105i). The laser beam is focused by a telescope-lens system into the center of the plasma source. The plane of polarization of the dye laser is perpendicular to the scattering plane.

The scattered radiation is detected perpendicularly to the laser beam crossing through the plasma source. The scattered light is collected by a system of two lenses and a Dove-prism used for rotating the image of the scattering volume to fit the 1m-monochromator (Spex, model 1704, grating 1200 lines/mm, blaze-wavelength 1 mm) entrance slit. In addition, a photomultiplier (RCA, type 4526, quantum-efficiency $\eta=20\%$ at $\lambda=400$ nm) at the exit is used. In order to reduce stray light to a tolerable level a diaphragm system with Brewster windows and a light dump for the laser beam were installed.

The multiplier was operated in a pulsed mode ($t_{ph}\approx 40$ ms) to prevent saturation effects by intense lines of the plasma source, which was running in a continuous mode. The scattering volume was 6×10^{-4} cm^3 (0.03 mm in width, 2 mm in height, and 10 mm in length) and the scattered radiation was collected by a solid angle $d\Omega=10^{-2}$ sr. Scattered light was measured during laser pumping at wavelengths in the vicinity of the selected spectral line by tuning the monochromator over this line including the far line wing where the photomultiplier output signal was very weak. Therefore, the multiplier signal was amplified by a factor of 100 with a preamplifier, the frequency band of which was 10 kHz $\leqslant \nu_{am} \leqslant 400$ MHz. A boxcar integrator (Stanford Research, type SR 250) recorded the signal of the scattered light with a gate period of $t_{bc}=50$ ns.

B. Plasma parameters

Spatially resolved, radial and axial measurements of the electron density and temperature were performed by using a Langmuir probe for different gas pressures 1 Pa$\leqslant p_g \leqslant$5 Pa and discharge currents 5 A$\leqslant I_d \leqslant$30 A [22]. From the probe measurements at the center of the plasma, we observed that electron density and temperature increase monotonically with increasing discharge current, and that the electron density increases with increasing gas pressure while the electron temperature decreases. Investigations of the variation of the plasmas parameters with the filling gas pressure indicate that for a gas pressure of $p_g=2$ Pa the plasma source shows a particularly stable and reproducible operation mode. The radial profiles of the electron density and electron temperature are presented in [22]. The measurements indicate, that for a small discharge current $I_d=5$ A the radial electron density profile is flat, but for discharge currents 10 A$\leqslant I_d \leqslant$30 A the density drops rapidly when moving away from the plasma center. In the radial range of $0\leqslant r_p \leqslant 2.5$ cm of the plasma column, there exists, within the error bars, a field-free plasma of high uniformity in the electron density range of 1.1×10^{12} cm$^{-3}\leqslant N_e \leqslant 1.6\times 10^{12}$ cm^{-3} and in the electron temperature range of 2.5 eV$\leqslant kT_e \leqslant$5 eV.

C. Operation of the plasma source for the redistribution of radiation observation

For operation of the plasma source the cathode was heated by a current of $I_c\approx 120$ A. The scattering experiments presented in the following were performed with a helium gas filling pressure $p_g=5$ Pa, a discharge current $I_d=20$ A and a discharge voltage $U_d\approx 100$ V, resulting in an electron density of $N_e=1\times 10^{12}$ cm^{-3} and an electron temperature of $kT_e=5$ eV at the discharge center; the uncertainty of the plasma parameters was found to be $\pm 20\%$.

In the scattering region the laser beam diameter was $d_l = 2$ mm. The energy of the beam before entering the discharge chamber was 0.5 mJ$\leqslant w_l \leqslant$1.8 mJ at a wavelength of the order of 400 nm. In the chamber it could not be measured. However, we proved experimentally that the fluorescence did not show any saturation effects by decreasing the incident laser power. The laser pulse duration was about 12 ns and the spectral width was 8 pm when employing Rhodamine 6G and Furan 2.

The experiment of Rayleigh scattering and redistribution of radiation was performed first by setting the dye laser wavelength to a chosen spectral distance (usually $\Delta\lambda = -30$ pm, 0 pm, 10 pm, 30 pm, 60 pm) from the center of the selected plasma line. The optogalvanic effect employing a helium lamp gave the reference for each line. Then the monochromator was tuned in steps of $\Delta\lambda = 4$ pm over the spectral line in question (observation of the lines was in second or third order). For every wavelength the scattering signals were averaged over about 300 dye laser pulses by the boxcar integrator. Its second window delayed slightly in time gave the background at each wavelength position. It was subtracted from the respective scattering signal. During the operational time of the experiment the laser output power was monitored by a photodiode and the plasma parameters of the source were controlled and held constant observing the discharge parameters voltage, current and filling pressure.

IV. MODELING THE RADIATIVE REDISTRIBUTION FUNCTIONS

A. Formalism

The theory developed in Mossé *et al.* [12] was designed to calculate line shapes of the fluorescence emitted by an optically active system immersed in a fluctuating thermal bath of perturbers (electrons and ions of the plasma) while being pumped by a monochromatic external radiation field. It is based on the frequency fluctuation model (FFM) [16]. Briefly, the plasma-emitter system is modeled, in the FFM, by partitioning it into an active radiating system and a perturbing bath. On the one hand, the perturbing bath is defined to be electric fields produced by the plasma particles (ions and electrons) which interact with the emitter modifying the radiated spectra. On the other hand, the radiative system is supposed to behave like a pseudomolecular system in this bath. The quantum mechanics for this pseudo-system is set up for static ion perturbers, while the electrons are treated in the impact approximation. This leads to a powerful renormalization process that creates a set of two-level Stark-dressed transitions (SDT). They are defined as the weakest observable resonant features that can be extracted from the quasistatic profile. Each SDT is characterized by the generalized complex frequency, $f_k - i\gamma_k$, and the generalized complex intensity, $a_k + ic_k$. The purely static profiles can be written as a sum of generalized Lorentzians. For the introduction of ion dynamics effects on the line shape or for the extension of the FFM to the radiative redistribution function calculations, a generalized dipole moment matrix element $(\mathbf{D}_k)_{eg}$ is defined. This can be done by relating the amplitude of the SDT dipole moment matrix element to the intensity of the transition associated with the coupling of the radiation field to the lower level g and the upper level e of the kth SDT. The normalized matrix element is $(\mathbf{D}_k)_{eg} = r\sqrt{1 + ic_k/a_k}$, where $r = \sqrt{\Sigma a_j}$ is the reduced matrix element of the transition associated with the emission of the SDT. To describe the instantaneous probability of occurrence of a particular SDT, the probability vector operator $\mathbf{p}$ is defined with element $p_k = a_k/r^2$.

The linear response line shape in the quasistatic ion/impact electron approximation can be written as an average over the initial and the sum over the final SDT in the extended Liouville space as

$$I(\omega) = \mathrm{Im} \sum_{i,f} p_i [\langle\langle \mathbf{D} | G^0(\omega) | \mathbf{D}\rho_0 \rangle\rangle]_{i,f}, \tag{3}$$

where

$$G^0(\omega) = (\omega \mathbf{1} - \ell_0)^{-1}, \tag{4}$$

and $\mathbf{1}$ is the unit operator. The Liouville operator ℓ_0 has a set of eigenfrequencies, $\omega_k = f_k - i\gamma_k$, composed of the generalized frequencies and widths of the SDT. Comparisons with other models, simulations and experiments have verified the accuracy of the FFM [23,24]. The one-photon line shape model above is extended now to the two-photon redistribution model by continuing the expansion of the response function to higher order in the emitter-radiation field interaction [25]. This approach is based on a previous investigation of the fluorescence of simple two- or three-level atomic systems in a plasma [17]. To calculate the spectrum of radiation scattered by an emitter in a plasma, one has to study the response of the atomic system perturbed by an external monochromatic electromagnetic field, observing the fluorescence radiation. On the one hand, the external field (laser field) that pumps the atomic system is treated classically by using the representation of harmonic numbers [26]. This method comes from the Floquet method [27], that makes it possible to remove the time dependence of the field interaction operator $\mathbf{V}_P$ which describes the coupling of the incoming pump radiation operator with the generalized dipole operator of the SDT. On the other hand, the fluorescence radiation is described as a spontaneous emission process of the SDT. In the following, $\mathbf{V}_S$ will be the field interaction operator for the coupling of the spontaneous emission with the generalized dipole operator of the SDT. Then, in this formalism, the power spectrum of the radiation emitted at frequency ω_S by a system pumped at frequency ω_P can be written as an average over the initial SDT and a sum over the final SDT, as

$$I(\omega_P, \omega_S) \propto \lim_{\eta \to 0} \mathrm{Im} \sum_{i,f} p_i (\langle\langle \mathbf{V}_S | \mathbf{G}(i\eta) | \mathbf{V}_P \rho_0 \rangle\rangle)_{i,f}. \tag{5}$$

The $\eta \to 0$ limit of the propagator in Eq. (5) is written as an operator in the extended space as

$$\mathbf{G}(\Omega) = [\Omega - \ell_0 - (\mathbf{V}_S + \mathbf{V}_P)]^{-1} \tag{6}$$

and satisfies the Dyson equation

$$\mathbf{G}(\Omega) = G^0(\Omega) + G^0(\Omega)(\mathbf{V}_S + \mathbf{V}_P)\mathbf{G}(\Omega), \tag{7}$$

where $G^0(\Omega)$ is given in Eq. (4).

The Dyson equation is developed to the lowest nonvanishing order. One obtains

$$I(\omega_P,\omega_S)\propto \mathrm{Im}\sum_{i,f} p_i(\langle\langle \mathbf{V}_S|G^0(\omega_S)\{\mathbf{V}_P G^0(\omega_S-\omega_P)\mathbf{V}_S G^0(-\omega_P)+\mathbf{V}_S G^0(0)\mathbf{V}_P[G^0(\omega_P)+G^0(-\omega_P)]\}|\mathbf{V}_P\rho_0\rangle\rangle)_{i,f}. \quad (8)$$

The first term in the curly bracket above gives the Rayleigh scattering line, centered on the frequency of the incident radiation ω_P. The second term describes the redistributed radiation.

As an application of this model, the feasibility of a resonant diffusion experiment, targeting a resonance between the $3d-2p$ line of Mg IV (14.6526 nm) and a Zr x-ray line at 14.6515 nm, was calculated and has been published elsewhere [13]. This frequency redistribution model was also used in the radiative transfer problem of amplifying media [6]. The spectral emissivity, corrected in order to account for redistribution of radiation, was calculated for lasers employing neonlike germanium and hydrogenlike carbon ions. In continuation of this study, investigations of the Doppler shift and the frequency redistribution function in the laboratory frame were performed recently using the above model [7].

B. Application of the formalism to the He I $2\,^3P-5\,^3D$ transitions

We present in this section an example of the calculation of the scattered spectra of the He I $2\,^3P-5\,^3D$ transitions using the previous formalism. The calculations are performed for the following plasma parameters $N_e=10^{12}$ cm^{-3} and $kT_e=5$ eV. For those given plasma parameters the electronic broadening is 0.3 pm. For the $2\,^3P-5\,^3D$ transition, there are six fine structure transitions and the effects of the states P, F, D and G of the level $n=5$ are taken into account. Five fine structure components are merging together, while the last one is still resolvable at $\Delta\lambda=16$ pm.

We performed calculations for different values of the pump field, i.e., for different wavelengths of the pumping laser. Figure 4 shows the scattered spectra as a function of the laser's wavelength separation from the resonance line at λ_0. Four examples are shown depending on the position of the pumping laser that are at $\Delta\lambda=+60$, $+50$, $+10$ and -30 pm from the resonance line. The scattered profiles are represented in log scale in order to emphasize the shape of the fine structure components and the Rayleigh lines.

V. RESULTS AND DISCUSSION

A. Measurements in the triplet system of He I

We observed partial redistribution on the $2\,^3P-5\,^3D$ transition at 402.6 nm. The signal was sufficiently intense to observe the spectra in 3rd order of the monochromator. The measured spectra were sufficiently described by 100 points over the wavelength window between $-50\leqslant\Delta\lambda\leqslant+80$ pm, where $\Delta\lambda$ is the frequency deviation from the line center. The scatter of the data points indicates the noise essentially due to the low signal levels.

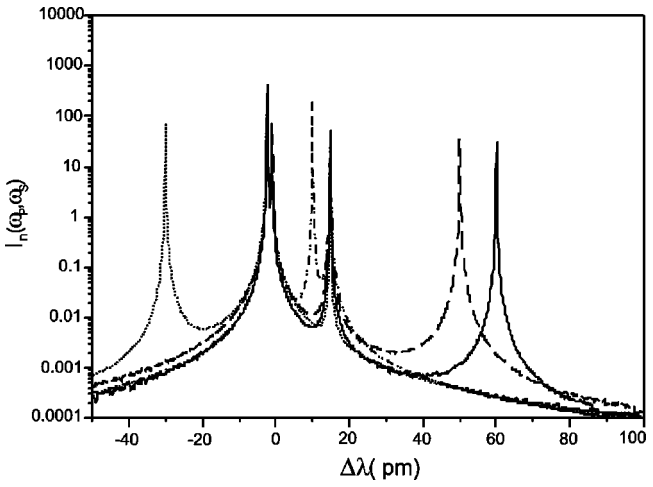

FIG. 4. Scattered spectra of the He I the $2\,^3p-5\,^3D$ transition at 402.6 nm calculated using the radiative redistribution model for different wavelengths of the pump laser: $\Delta\lambda=(\lambda_p-\lambda_0)=+60$ pm (full line), $\Delta\lambda=+50$ pm (dashed line), $\Delta\lambda=+10$ pm (dot-dashed line), and $\Delta\lambda=-30$ pm (dotted line).

We have investigated many positions of the pumping laser from the red wing to the blue one of the line ($\Delta\lambda_P=+60$, $+30$, 0, -30 and -60 pm). The apparatus function was measured to have a Gaussian shape with a FWHM (full width at half maximum) of 26 pm. Each calculated spectrum was convolved with this profile. For the comparisons of these calculated spectra with the measured ones, we also fitted first each experimental spectrum with two Gaussian profiles of the above FWHM. One Gaussian profile was centered on the wavelength of the pumping laser wavelength (Rayleigh peak), and the other one was centered on the resonance line (fluorescence line). Then, we adjusted the maximum intensity of the fluorescence part of the theoretical spectrum to the latter Gaussian profile. We thus could check if the Rayleigh part of the theoretical spectrum was in agreement or not with the measured one. With this procedure, we were able to check the reliability of the calculated electron collisional broadening. Nevertheless, due to the very broad apparatus function compared to the other broadening mechanisms, the effect of the electron-atom *inelastic* collisions could be not investigated and, therefore, was neglected in the calculations. Only the electron-atom *elastic* collision rates γ_e, calculated as discussed in Sec. II, were taken into account.

As an illustration, we present in Fig. 5 a comparison between the measured spectrum of the $2\,^3P-5\,^3D$ transition and the theoretical one, for a pumping laser set at $\Delta\lambda=+60$ pm from the line center. As reference, the calculated scattered spectrum before the convolution accounting for the Doppler broadening and the apparatus function is also given in this figure. The calculated scattered spectrum shows very good agreement with the measured one within the error bars. We have checked the influence of a variation of γ_e on the redistribution profile, and a variation higher than $\pm20\%$

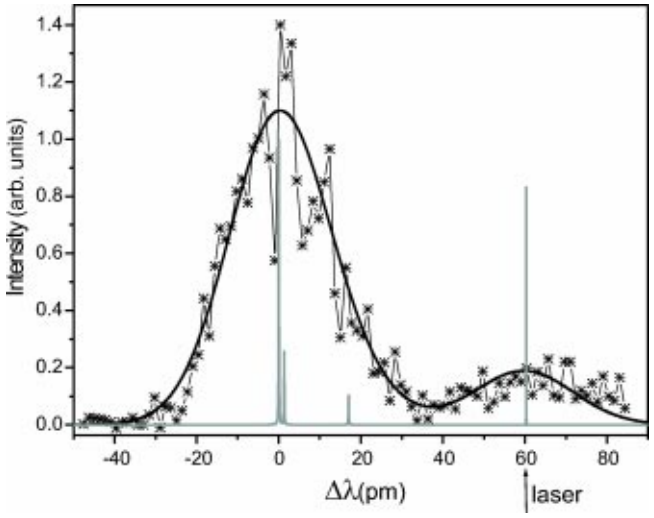

FIG. 5. Comparison between the measured (crosses) and calculated (line) scattered spectrum of the He I $2\,^3p$–$5\,^3D$ transition at 402.6 nm for a pumping laser at $\Delta\lambda = +60$ pm from the line center. [The pure electron broadened redistribution spectrum before convolution with a Gaussian profile (FWHM = 26 pm) is shown in gray.]

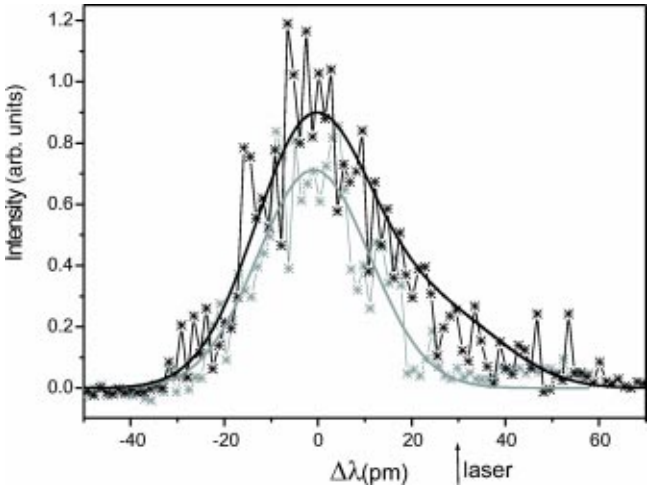

FIG. 7. Comparison between the measured (black crosses) and calculated (black line) scattered spectrum of the He I $2\,^3P$–$5\,^3D$ transition at 402.6 nm for a pumping laser at $\Delta\lambda = +30$ pm from the line center. As reference the measured spectrum without pumping is shown (gray crosses) and its fit with a Gaussian profile (FWHM = 26 pm; gray line).

would lead to disagreement between the measured and the theoretical scattered spectra as it is shown in the Fig. 6.

By comparing a spectrum with and without the pumping laser effect, we show in Fig. 7 how the redistribution of radiation is effective. For the pumping laser set at $\Delta\lambda = +30$ pm from the line center, the fluorescence intensity is increased by a factor of 1.3 compared to the signal measured without the pumping laser.

Partial redistribution was observed also on the $2\,^3P$–$4\,^3S$ transition at 471.3 nm, as was predicted theoretically. The scattered spectra were measured in second order and the calculated spectra were convolved with a Gaussian profile of a width found to be equal to 37.3 pm. Figure 8 gives an example of such an observed partial redistribution case, while the transition is pumped at $\Delta\lambda = -40$ pm from the line center. The calculated scattered spectrum is found to be in relatively good agreement with the observed one.

The characteristics of the $2\,^3P$–$4\,^3D$ transition at 447.2 nm correspond to case IV in Fig. 2. As theoretically predicted, we should observe a dominance of the Rayleigh peak. Unfortunately, no conclusion can be drawn since the three experimental spectra (recorded for a pumping laser set at $\Delta\lambda = -30, +20, +30$ pm) show no variation whatever with the laser wavelength.

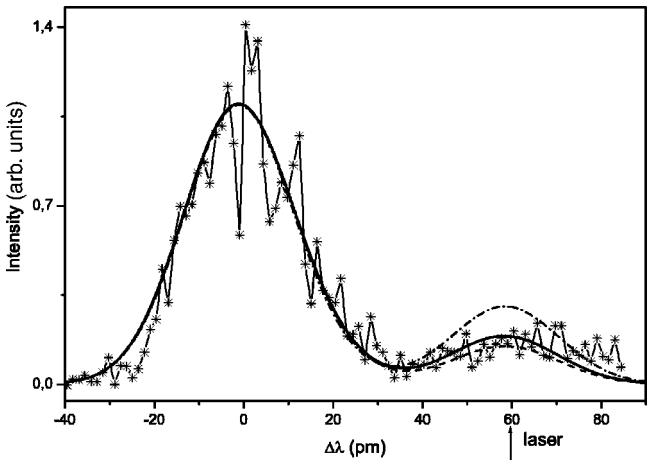

FIG. 6. Calculated scattered spectra of the He I $2\,^3p$–$5\,^3D$ transition at 402.6 nm compared to the measured one (crosses) for different values of the elastic collision rate. The full line spectrum is the result using γ_e. The dashed line corresponds to a calculation with ($\gamma_e = +20\%$); the dot-dashed line is for ($\gamma_e = -20\%$). The pumping laser is set at $\Delta\lambda = +60$ pm from the line center.

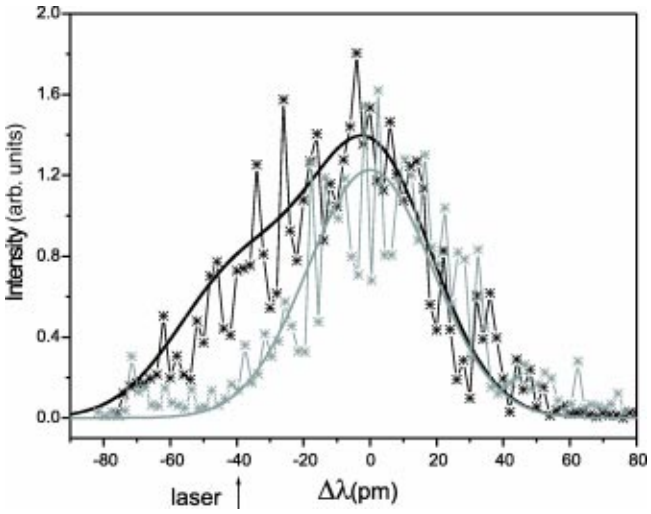

FIG. 8. Comparison between the measured (black crosses) and calculated (black line) scattered spectrum of the He I $2\,^3P$–$4\,^3S$ transition at 471.3 nm for a pumping laser at $\Delta\lambda = -40$ pm from the line center. As reference the measured spectrum without pumping is shown (gray crosses) and its fit with a Gaussian profile (FWHM = 37.3 pm; gray line).

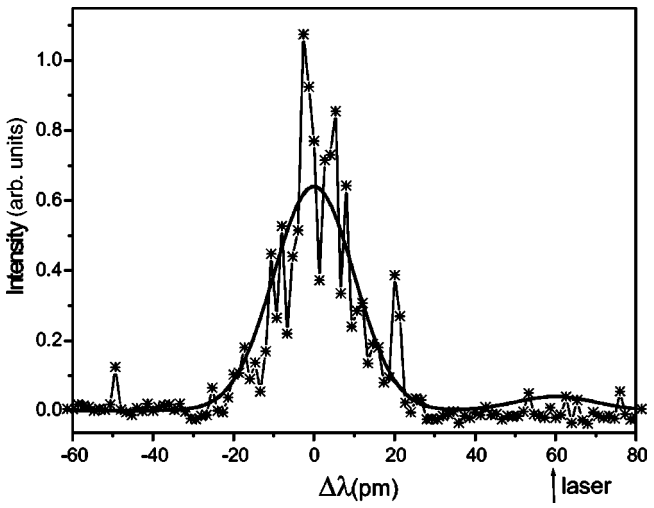

FIG. 9. Comparison between the measured (crosses) and calculated (black line) scattered spectrum of the He I $2\,^1S-4\,^1P$ transition at 396.5 nm for a pumping laser at $\Delta\lambda=+60$ pm from the line center. The calculated spectrum was convoluted with a Gaussian profile with a FWHM=20.5 pm.

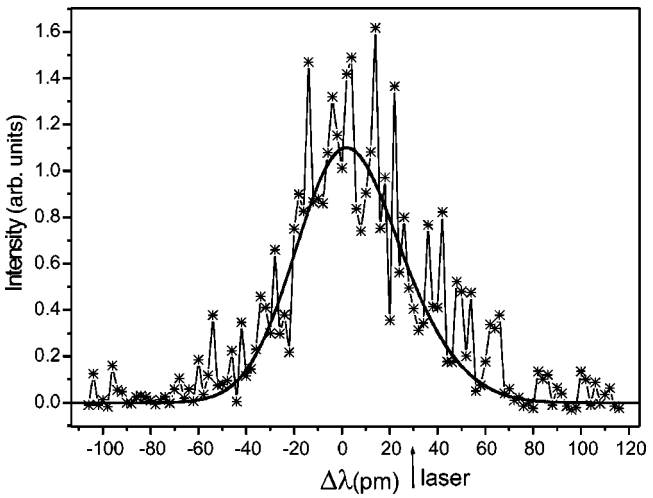

FIG. 10. Comparison between the measured (crosses) and calculated (black line) scattered spectrum of the He I $2\,^1P-5\,^1D$ transition at 438.8 nm for a pumping laser at $\Delta\lambda=+30$ pm from the line center. The calculated spectrum was convoluted with a Gaussian profile with a FWHM=44.5 pm.

B. Measurements in the singlet system of He I

The same procedures have been used to investigate redistribution of radiation on transitions in the singlet system of He I. Measurements of the scattered radiation have been done in third order for the $2\,^1S-4\,^1P$ transition, while measurements on the $2\,^1P-5\,^1S$ transition were carried out in second order, due to the very low intensity signal. Figures 9 and 10 show results of those lines. In the case of the $2\,^1S-4\,^1P$ transition, the measured spectrum reveals a small bump at the position of the Rayleigh peak. Nevertheless, no conclusions can be drawn concerning the agreement with the theoretical scattered spectrum since the signal to noise ratio is very poor. On the scattering signal of the $2\,^1P-5\,^1S$ transition we observed an asymmetry of the profile while pumping at $\Delta\lambda=+30$ pm from the line center (see Fig. 10).

VI. CONCLUSION

We present experimental observation of Rayleigh scattering and redistribution of radiation and independently calculated profiles where the width is given by experimental conditions. The theoretical profiles in the graphs reveal good agreement with the experiment. Changing the electron collisional rate by more than 20% leads to observable deviation. We conclude, therefore, that the elastic collisional rate and our model for calculation of radiative redistribution describe well the situation at the prevailing plasma conditions. Further experiments with higher resolution are certainly desirable to provide a test-bed for this model and therefore to employ it as a diagnostic tool.

ACKNOWLEDGMENTS

The authors are grateful to Dr. W. Eissner for his calculations of the atomic data of He I. It is also a pleasure to acknowledge stimulating conversations with Dr. C. Mossé, Dr. A. Calisti, and Dr. B. Talin, from Université de Provence, Marseille, France, and the advice of Professor H. F. Döbele and his group on the magnetic multipole source. This work was supported by the Deutsche Forschungsgemeinschaft and by the SFB 191.

[1] S. Chandrasekhar, *Radiative Transfer* (Dover, New York, 1960).
[2] D. Mihalas, *Stellar Atmospheres*, 2nd ed. (Freeman, New York, 1978).
[3] J.B. Yelnik and D. Voslamber, Astrophys. J. **230**, 184 (1979).
[4] V. Bommier, Astron. Astrophys. **328**, 706 (1997).
[5] A. Omont, E.W. Smith, and J. Cooper, Astrophys. J. **175**, 185 (1972); **182**, 283 (1973).
[6] D. Benredjem, C. Mossé, H. Guennou, A. Sureau, A. Demir, B. Talin, and C. Möller, J. Phys. B **33**, 2295 (2000).
[7] D. Benredjem, C. Mossé, B. Talin, and C. Möller, J. Phys. B **34**, 1369 (2001).
[8] J.L. Carlsten and A. Szöke, J. Phys. B **9**, L231 (1976); Phys. Rev. Lett. **36**, 667 (1976).
[9] S. Maurmann, Dissertation, Ruhr Universität Bochum, 1984.
[10] G.G. Lombardi, D.E. Kelleher, and J. Cooper, Astrophys. J. **288**, 820 (1985).
[11] G. Himmel and L. Sowa, J. Phys. B **16**, 4117 (1983).
[12] C. Mossé, A. Calisti, R. Stamm, B. Talin, R.W. Lee, and L. Klein, Phys. Rev. A **60**, 1005 (1999).
[13] C. Mossé, A. Calisti, M. Koubiti, R. Stamm, B. Talin, J. Koch, R.W. Lee, and L. Klein, J. Quant. Spectrosc. Radiat. Transf. **55**, 439 (1996).
[14] P. Drepper, dissertation, Ruhr Universität Bochum, 2000.

[15] A. Calisti, L. Godbert, R. Stamm, and B. Talin, J. Quant. Spectrosc. Radiat. Transf. **51**, 59 (1994).
[16] B. Talin, A. Calisti, L. Godbert, R. Stamm, L. Klein, and R.W. Lee, Phys. Rev. A **51**, 1918 (1995).
[17] B. Talin, R. Stamm, V. Kaftandjian, and L. Klein, Astrophys. J. **322**, 804 (1987).
[18] C. Theodosiou, At. Data Nucl. Data Tables **36**, 97 (1987).
[19] H. Griem, M. Blaha, and P. Kepple, Phys. Rev. A **19**, 2421 (1979).
[20] R.K. Janev, W.D. Langer, K. Evans, Jr., and D.E. Post, At. Mol. Proc. Hydrogen-Helium Plasmas **PPL-TM 157**, 203 (1985).
[21] T. Lokajczyk, dissertation, Ruhr Universität Bochum, 1997.
[22] S. Maurmann, P. Drepper, S. Ferri, and N. Petershagen, Contrib. Plasma Phys. **40**, 152 (2000).
[23] B. Talin, A. Calisti, S. Ferri, M. Koubiti, T. Meftah, C. Mossé, L. Mouret, R. Stamm, S. Alexiou, R.W. Lee, and L. Klein, J. Quant. Spectrosc. Radiat. Transf. **58**, 953 (1997).
[24] L. Godbert-Mouret, T. Meftah, A. Calisti, R. Stamm, B. Talin, M. Gigosos, V. Cardenoso, S. Alexiou, R.W. Lee, and L. Klein, Phys. Rev. Lett. **81**, 5568 (1998).
[25] B. Talin and L. Klein, Phys. Rev. A **26**, 2717 (1982).
[26] A. Ben-Reuven and Y. Rabbin, Phys. Rev. A **19**, 2056 (1979).
[27] J.H. Shirley, Phys. Rev. **138**, B979 (1965).